Clean Energy, 2022, Vol. 6, No. 5, 776–786
https://doi.org/10.1093/ce/zkac039
Advance access publication 1 November 2022
Research Article

Experimental study on the optimum design of diffuser-augmented horizontal-axis tidal turbine

Evi Elisa Ambarita, Harinaldi*, Rifqi Azhari and Ridho Irwansyah

Department of Mechanical Engineering, Universitas Indonesia, Kampus UI Depok 16424, Indonesia

*Corresponding author. E-mail: harinald@eng.ui.ac.id

Abstract

Ocean current energy is a promising and reliable resource that offers sustainability and predictability in realizing green future needs. A diffuser-augmented horizontal-axis turbine is utilized to generate ocean current energy. A numerical study on the impact of diffuser angle variations on the power coefficient has been carried out in the previous research. To elucidate the fluid dynamics aspects and further validation of previous computational results, the experimental investigation on the optimal design of tidal turbine with 20.04° diffuser augmentation is presented in this study. The study was conducted in a flowing tank with a current velocity of 0.7 m/s. The maximum power coefficient of 20.04° is 0.436 experimentally, which is a little smaller than the numerical value. Moreover, to reinforce the 20.04° result, a diffuser with an angle of 10.43° was also manufactured and tested experimentally. The maximum power coefficient of 10.43° is 0.303 experimentally, which is 3% smaller than the numerical value. It was concluded that the numerical approach might be considered satisfactory and represent similar phenomena to the experimental investigation in an application for modelling of multi-objective optimization.

Graphical Abstract

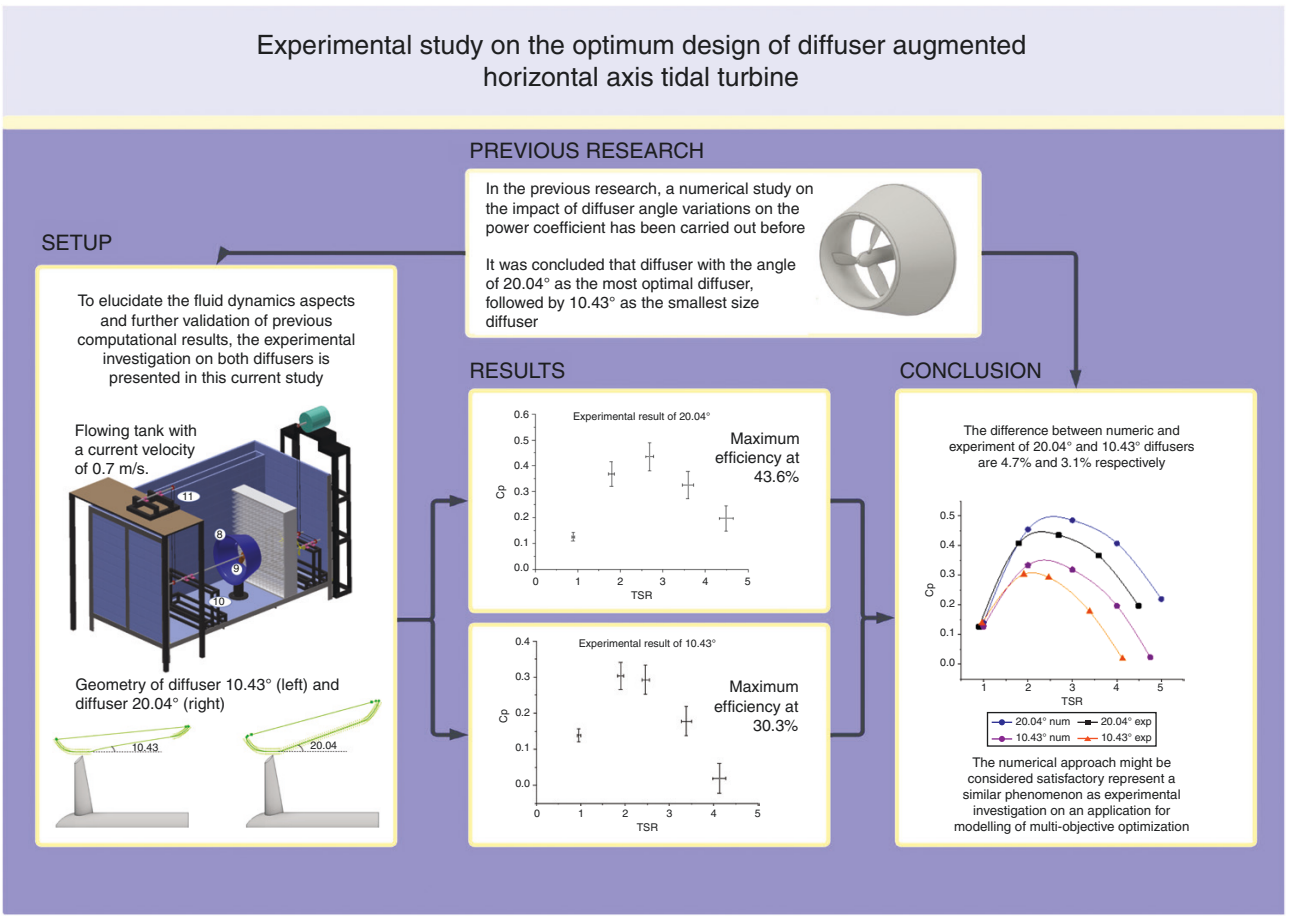

Keywords: ocean current energy; tidal turbine; diffuser augmentation; power coefficient; experimental study

Received: 6 February 2022. **Accepted:** 21 June 2022

Introduction

Renewable energy is expected to play a significant role in meeting green future needs while reducing environmental pollution and climate change [1]. Since ~70% of Earth's surface is covered by oceans, ocean current is a promising resource to generate large amounts of energy [2] with an estimated 307 GW by 2050 [3]. There are several different ocean renewable energies: wave energy, tidal energy and ocean current energy [4]. Ocean current technology is one of the most recent forms of renewable energy to be developed as it offers sustainability and predictability [5]. Moreover, the implementation of ocean current energy would support sustainable growth by lowering the negative impact on the biosphere while remaining environmentally friendly [6]. Many devices are being studied for ocean current energy conversion although most are designed around the underwater turbine [7].

There have been a few published studies concerning the exploitation of tidal turbines around the world both numerically and experimentally. Some studies even claimed that to increase the turbine power output, a diffuser augmentation is an excellent option in both wind and tidal turbines [8–10]. The power produced by a tidal turbine is directly proportional to the cube of the incoming current velocity; thus, even a slight increase in velocity increases the power significantly [11]. The augmentation available from ducting comes from an increased mass flow rate, which increases the flow velocity at the rotor plane. The main mechanism for increasing the mass flow rate is a reduction in the pressure, at both the rotor plane and the diffuser exit, to below that which would be possible to be sustained for a bare turbine. This pressure reduction causes the additional flow to be drawn into the duct. Since the cross-sectional area of the duct is fixed at the rotor, continuity means that an increase in the mass flow rate causes an increase in the flow velocity [12]. The pressure drop available for a ducted turbine depends on the duct shape and the flow through and over it. If the duct has a shape like a diffuser, it attracts more fluid through it and intensifies the available pressure drop over the turbine by restoring some of the velocity head downstream as the pressure head [13]. Thus, a diffuser acts as a flow amplification device by increasing the mass flow rate, thereby accelerating the incoming current velocity, which results in an appreciable increase in the power output for extraction by the rotor. Therefore, the turbine efficiency is remarkably advanced by a diffuser [14]. Mehmood *et al.* investigated a study of NACA 0015 for diffuser design in tidal current turbine applications and concluded that diffuser augmentation increased the inlet velocity by ~165%, from 1.2 to 3.18 m/s [15]. In a separate report, Mehmood *et al.* also explored a study of a diffuser-augmented tidal turbine with NACA 0028. The work reported that the inlet velocity increased by ~141%, from 1.5 to 2.9 m/s [16]. Elbatran *et al.* examined a prototype of a four-blade augmented-diffuser tidal turbine applying NACA 0014 and found that the power coefficient increased by ≤1.7 times with the maximum power output increasing from 166 to >249 W [13]. Shahsavarifard investigated the effect of a shroud on the performance of horizontal-axis hydrokinetic turbines and concluded that the maximum power increased by 91% over the unshrouded turbine [17]. Through numerical and experimental analysis of a diffuser-augmented micro-hydro turbine, Song *et al.* verified that the diffuser-augmented turbine enhanced output power by ~27% with respect to the bare turbine [18]. Sun and Kyozuka clearly found that the diffuser-augmented turbine achieved a maximum power coefficient of ≤2.5 times that of the bare turbine [19, 20].

Yet, there are several principal differences in the modelling, such as in the design of the diffuser augmentation, and the working of the turbine design amongst those studies, which would demand further research and investigation. By applying multi-objective optimization, Ambarita *et al.* computationally declared that a diffuser angle of 20.04° was the optimal diffuser-augmented tidal turbine design [21, 22], which was in accordance with the study by Sakaguchi and Kyozuka [23]. Ambarita *et al.* applied the governing equations carried out by Zhang *et al.* [24, 25], which were experimentally presented by Bahaj *et al.* [26, 27]. To elucidate the fluid-dynamic aspects and further validation of previous computational results [22], this current study will experimentally investigate the performance of a tidal turbine with 20.04° diffuser augmentation. This test is carried out in a flowing tank with artificial currents and several approaches. It investigates the effect of the diffuser on the inlet velocity before hitting the rotor blades. The difference in the power coefficient between numerical and experimental results is also discussed.

1 Numerical method

Since the computational method has been presented in a previous report, only the summary is explained here. Further details can be found in Ambarita *et al.* [22]. Computational fluid dynamics (CFD) was used that was based on the Reynolds-averaged Navier–Stokes (RANS) equations for the conservation of mass and momentum. The CFD model refers to the governing equations of simulation conducted by Zhang *et al.* [24, 25]. A 1/2 scale model with three blades based on the NACA 4616 airfoil and a rotor diameter of 0.3 m was numerically examined in a steady-state and k-epsilon (k-ε) turbulence model [22]. The turbine model is shown in Fig. 1a and the 3D model for better visualization in Fig. 1b, in which θ represents the diffuser angle of 20.04°. The modelled inlet velocity was 0.7 m/s with a tip speed ratio (TSR) ranging from 1 to 5. The multi-reference-frame model was used for the CFD model in which individual cell zones can be assigned different rotational speeds [28].

The adapted numerical method was based on a combination of the CFD model and multi-objective optimization. The CFD model was used to analyse turbine performance by considering the power coefficient and cavitation inception that caused it. The multi-objective optimization was utilized to discover the optimal diffuser angle design of the tidal turbine that has the maximum power coefficient and the minimum cavitation risk.

In a previous study, the tests were carried out on the diffuser with seven angles, namely 10.43°, 15.34°, 20.04°, 24.46°, 28.6°, 32.44° and 35.97°. It was concluded that the larger the diffuser angle, the higher the power coefficient, yet the higher the cavitation risk. The diffuser angles with the highest and lowest power coefficients corresponded to diffuser angles of 35.97° and 10.43°, respectively [21, 22]. By multi-objective optimization, the optimal design of a horizontal-axis tidal turbine corresponded to a diffuser angle of 20.04°, which was in agreement with the study by Sakaguchi and Kyozuka [23]. Therefore, in this study, the optimum diffuser angle of 20.04° and the turbine device were manufactured to be tested experimentally to validate the power coefficient of the numerical study. Moreover, the diffuser angle of 10.43° was also manufactured and tested to reinforce the result and validation of 20.04°. The angle of 20.04° was chosen as the optimal design and the 10.04° angle was selected as the smallest angle to simplify the manufacturing and experimental process in terms of low cost.

1.1 Rotor geometry

The rotor geometry was created to be representative of previous work [19–23] whilst remaining as simple as possible for ease of modelling and construction. A 0.3-m rotor diameter with three

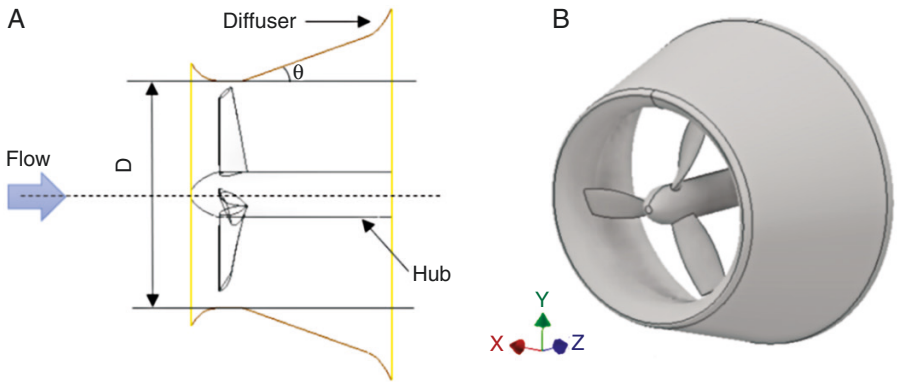

Fig. 1: (a) The geometry model of a horizontal-axis tidal turbine; (b) 3D model with the diffuser's thickness [21, 22].

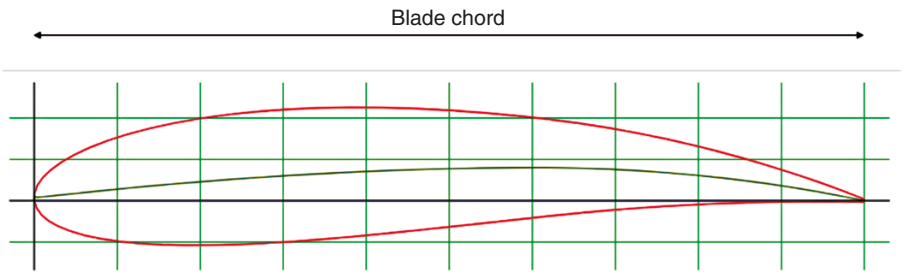

Fig. 2: NACA 4616 (source: http://airfoiltools.com).

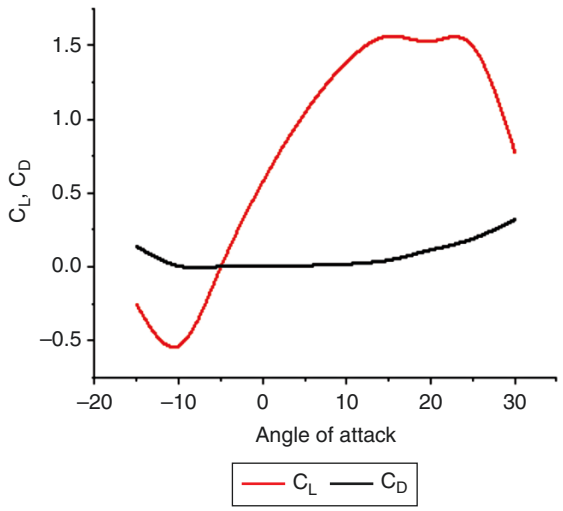

Fig. 3: Lift and drag coefficients of NACA 4616 at a Reynolds number of 5×10^5.

blades was manufactured. The blades were developed from a NACA 4616 blade section as shown in Fig. 2. The lift and drag coefficients against the angle of attack at a Reynolds number of 5×10^5 obtained through Xfoil are shown in Fig. 3. The details of the blade design, with the ratio of the blade length (r) and total blade length (R), can be seen in Table 1. This current study is only focused on one type of airfoil. A different airfoil type of rotor blade is in the process of investigation, which will be reported in a separate study.

1.2 Diffuser geometry

The diffuser geometry was designed following previous works [22, 23] by multi-objective optimization using a genetic algorithm-artificial neural network (GA-ANN). The inlet and outlet diameters of the 10.43° diffuser are 0.3 and 0.4 m, respectively, whereas in the 20.04° diffuser, the inlet and outlet diameters are 0.3 and 0.5 m, respectively. Fig. 4 shows the final experimental geometry in cross section along the shaft length. A view of the combined rotor and diffuser in design can be seen in Fig. 1.

Table 1: Blade geometry details for the experimental blade sets

r/R	Angle of attack (degrees)	Stagger angle (degress)	Twist (degrees)
0.1	23.48	23.53	0
0.3	20.37	45.95	17.56
0.5	14.09	60.36	36.83
0.7	10.34	65.02	40.16
1.0	7.51	69.96	45.43

2 Experimental procedure

2.1 Test facilities

The experiments were conducted in the flowing tank as seen in Fig. 5 at the fluid mechanic laboratory, Universitas Indonesia, with a water level of 0.8 m. The maximum blockage in the flowing tank, when the rotor and diffuser were run together, results in a channel wall blockage of 0.206 for the 20.04° design and of 0.176 for the 10.43 ° design. These blockages due to the limited facilities have been considered for analysing the turbine performance [29].

The inlet velocity was metered using a current meter, which was of the propeller type. This meter utilizes propellers to sense velocity that is rated by dragging them through tanks of still water at a known speed. The accuracy of the current meter is estimated to be ±5%. The measurement of the inlet velocity was conducted in two locations, namely in the front and inside the diffuser-augmented device, to investigate the effect of the diffuser.

While measuring, the position of the propeller hub must be perpendicular to the inflow, then the current velocity in m/s will be read on the screen of the current meter.

To create the artificial current, two ship propellers driven by a 2.2-kW electric motor were used that were coupled by a pulley-and-belt system as seen in Fig. 5 with legends 3, 6 and 7. The rotating propellers also led the current to circulate from the large area to the narrow area of the flowing tank as indicated by the red arrow in Fig. 5, thereby avoiding backflow. Water flowing through propellers will hit the turbine blades resulting in a rotating rotor. A straightener with a channel diameter of 10 mm was set 0.2 m in front of the turbine to straighten the flow before hitting the turbine. Across the flow field domain of this experimental set-up, the uniformity of upstream flow has an average inlet velocity of 0.72 m/s with a deviation of ±0.2 m/s, which is believed to be sufficiently representative for the measurement of the power coefficient and comparable enough to justify numerical results.

2.2 Models

The general arrangement of 20.04° and the turbine rig can be seen in Fig. 6. The blades were fabricated using a 3D printer with a printing layer thickness of 0.1 mm. The filament was polylactide (PLA) plastic. To achieve the surface finish perfectly, the blades were polished using sandpaper until smooth. The final geometry of the rotor blades follows the design. The hub was made of aluminium with a front diameter of 60 mm and a rear diameter of 15 mm. The diffusers of 10.43° and 20.04° were manufactured. Both diffusers were made of 4-mm plywood that was laser-cut and resin was added to shape the diffuser, which was then coloured using oil paint.

2.3 Experimental set-up

The key features of the experimental set-up can be seen in Fig. 7. To avoid any measurements in the water, the power transmission system is conducted through a pulley and belt. This system with a V-belt type A has an efficiency of 75% [30], which has been taken into account for evaluating the turbine torque. The pulley under the water is coupled to the turbine hub. The other pulley over the water is coupled to another shaft. Those two pulleys are connected by a V-belt. The measurement is carried out on the shaft over the water. The shaft is linked to a breaker and load cell sensor. A breaker is used to vary the rpm at the desired TSRs according to the numerical method. The load cell sensor is connected to the computer using NI USB-6211. The test is conducted

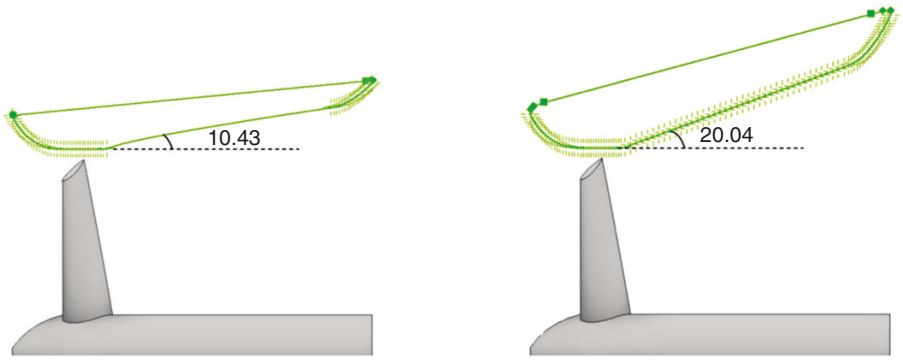

Fig. 4: Cross section of the diffuser shape along the shaft length. (a) 10.43°; (b) 20.04°.

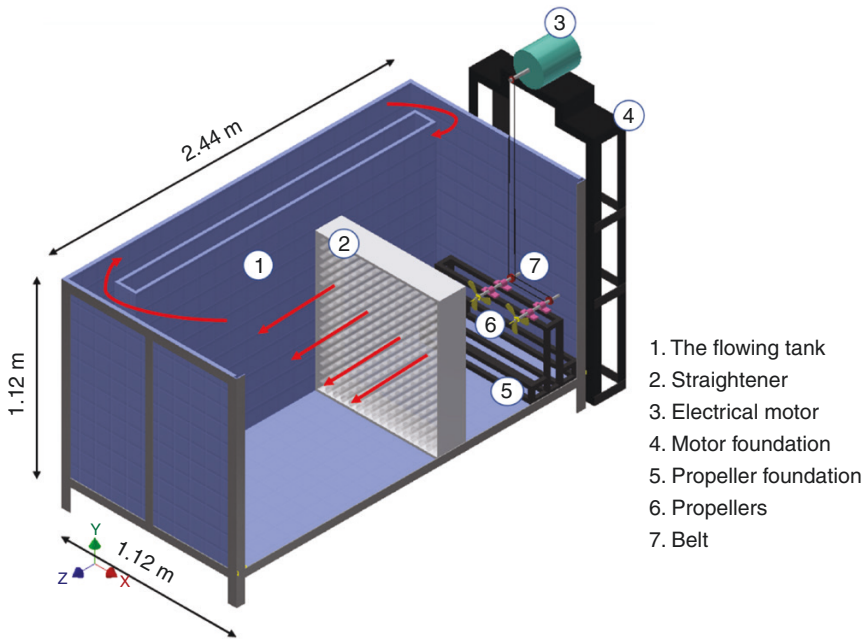

Fig. 5: Visualization of the flowing tank.

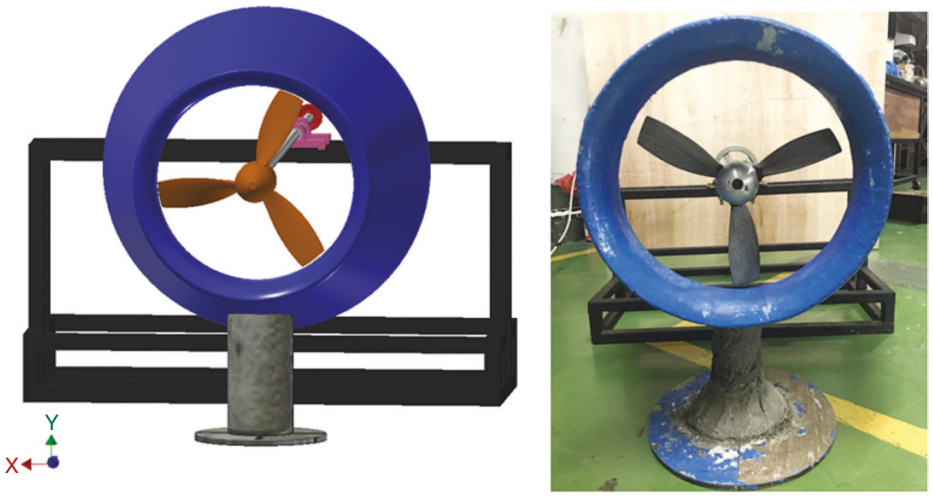

Fig. 6: Details of the turbine device displaying the geometry and assembly of 20.04. (a) Computer-aided design model; (b) the manufactured photograph.

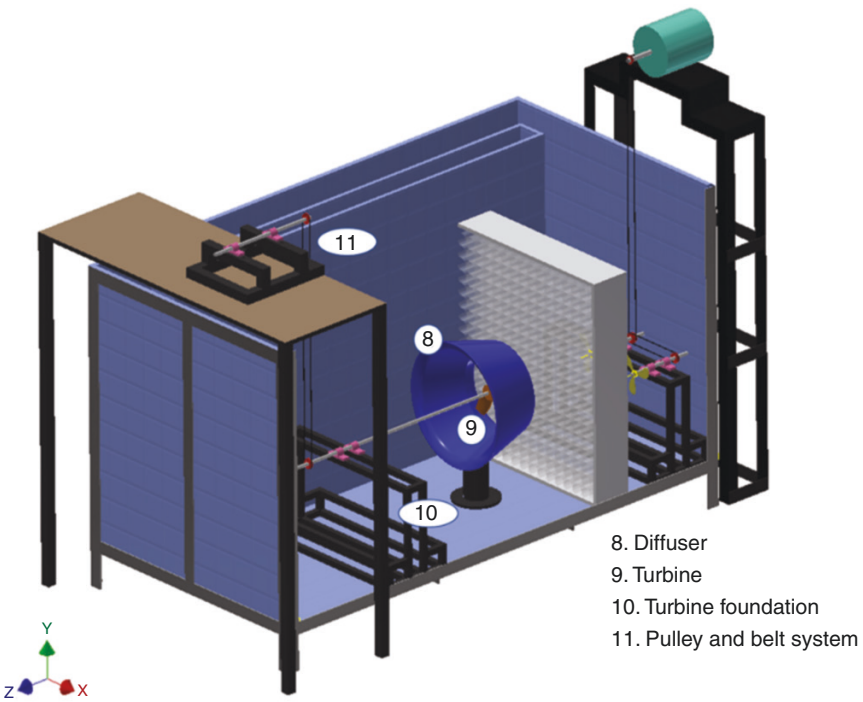

Fig. 7: The experimental set-up.

to evaluate the power coefficient of the turbine with variations of TSR. As a numerical method, TSR ranged from 1 to 5 resulting in variations of the blade angular speed from 44 to 222 rpm.

2.4 Data collection process

This method utilizes three measuring tools, i.e. a tachometer to read rpm, a load cell to measure the torque and a current meter to measure the flow velocity. The contact tachometer type works by bringing a freely spinning wheel into direct contact with the rotating object. The DT-6236B tachometer has autoranging with 0.05% accuracy.

The torque measurement uses a load cell with the maximum load of 500 g, a load cell amplifier, NI USB-6211, using a 16-bit microcontroller and a power supply. NI USB-6211 is simpler and less inexpensive for this work. Since the voltage generated by the load cell is low, an amplifier is required to increase the voltage. The power supply uses as a resource the load cell amplifier. The layout of the measuring instruments for collecting data is presented in Fig. 8.

As the load cell produces voltage and NI USB-6211 is able to read the voltage, then the use of NI USB-6211 is suitable for this work. To obtain the result in torque (Nm) as shown in Equation 1, the relationship between voltage and various masses is used:

$$\tau = F.r = m.g.r \tag{1}$$

where τ represents the torque (Nm); and m, g and r represent the mass (kg), gravitational acceleration (m/s^2) and radius (m), respectively.

For the data collection, first the turbine device and the measurement tools are set up in the proper position as seen in Fig. 9 with the legend described in Figs 5 and 7. The electric motor is plugged into the power source to drive the two ship propellers

resulting in the artificial currents, then the current is allowed to stabilize. The current meter is utilized to measure the flow velocity located between the straightener and the turbine. Next, the data collecting process is started. The turbine shaft is braked using a breaker until the desired rpm is reached. The rpm is measured using a tachometer. On the computer, the NI software is run then the voltage data read by NI USB-6211 is saved. The voltage data are converted to the mass using the calibration equation that has been presented. In the end, the torque can be calculated using Equation (1). To find the power coefficient graph, the steps above are repeated with variations of rpm.

For a given average flow velocity, the torque (τ) and rotational speed (ω) are used to calculate the power coefficient (C_p), which can be determined and mathematically expressed as:

$$C_P = \frac{\tau\ \omega}{0.5\rho AV^3} \tag{2}$$

where A represents the cross-sectional area of the turbine (πR^2) and V represents the inlet velocity (m/s). In the experimental method, an uncertainty analysis is required. Each measuring tool has its own uncertainty (u), namely load cell of 2.56%, tachometer of 2.5% and current meter of 2.5%.

3 Results

3.1 Diffuser characteristics

To understand the behaviour of the combined diffuser and turbine device, it is first necessary to understand the flow through the empty diffuser. Due to a narrowing of the area before hitting the turbine, the current velocities ahead and inside the diffuser are significantly different. The current flowing before and through the diffuser was experimentally measured to check the effect of the diffuser. The current meter was utilized for the direct measurement of the current velocity. Fig. 10 shows the locations at which the current velocity was measured before entering the diffuser. These data are not taken at the same time but are measured alternately from point to point.

The value for each position is also shown in Fig. 10 and the average velocity is 0.72 m/s. Then the current velocity inside the diffuser was experimentally measured up to 1 m/s. Since the cross-sectional area of the diffuser was fixed at the rotor, continuity means that an increase in the mass flow rate causes an increase in the flow velocity.

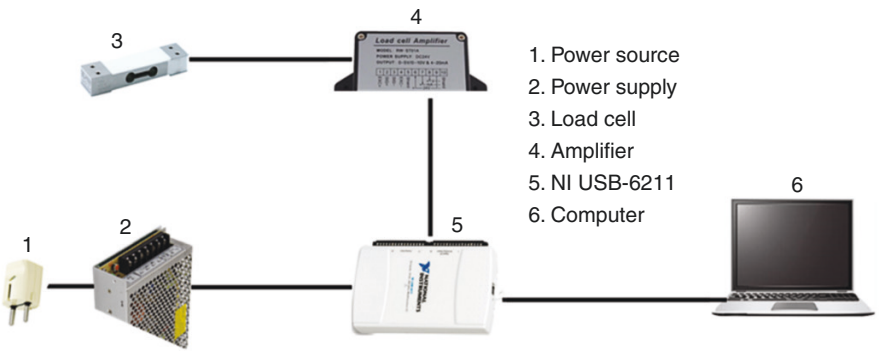

Fig. 8: The layout of measuring instruments for collecting data.

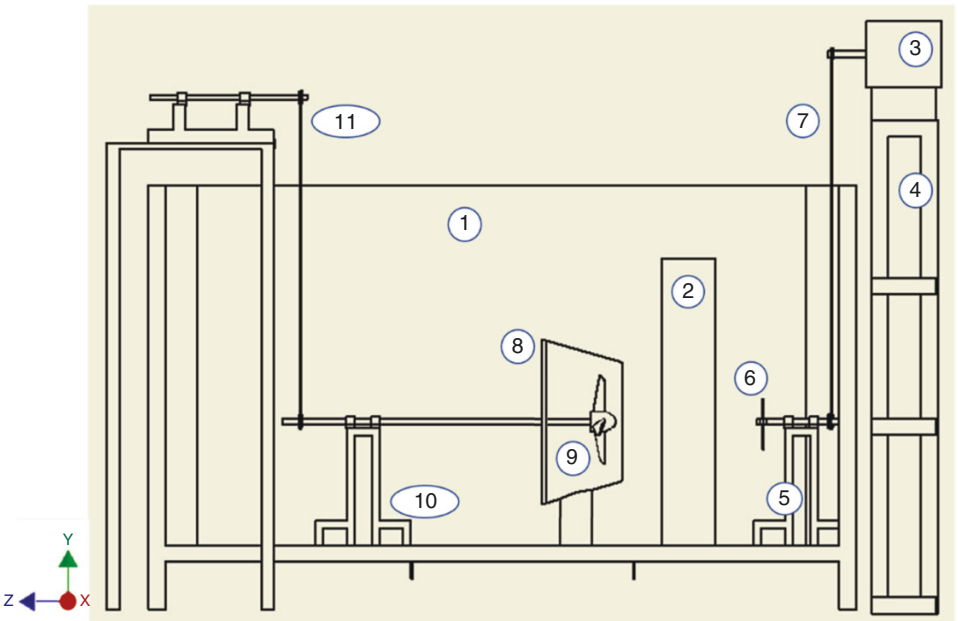

Fig. 9: The schematic of the experimental set-up.

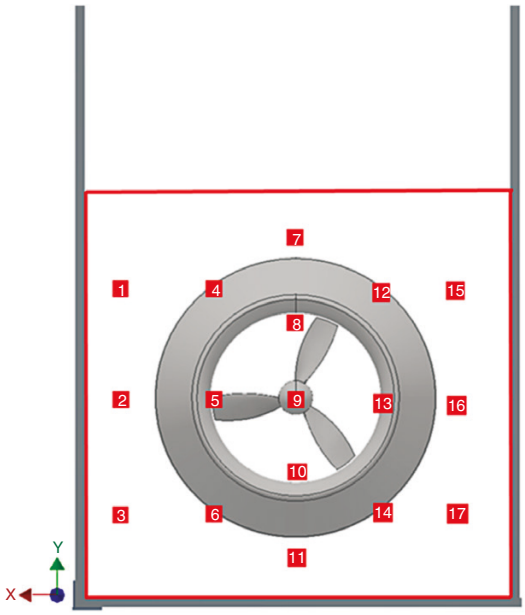

Position	Velocity (m/s)
1	0.7
2	0.8
3	0.7
4	0.75
5	0.82
6	0.77
7	0.76
8	0.8
9	0.82
10	0.81
11	0.75
12	0.7
13	0.8
14	0.7
15	0.5
16	0.5
17	0.5
Average	0.72

Fig. 10: The current velocity measured before entering the diffuser.

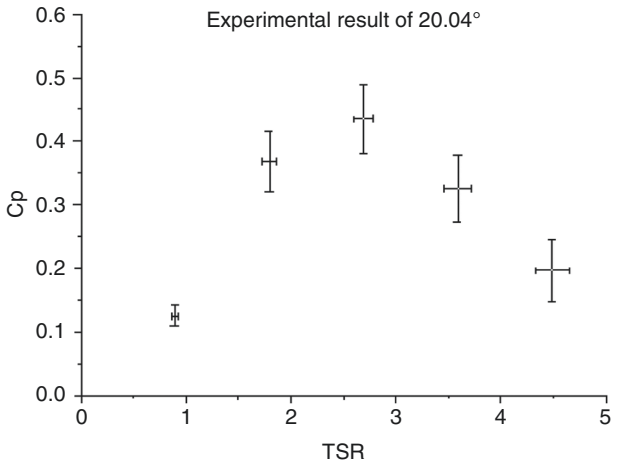

Fig. 11: The power coefficient of the experimental result as a function of the tip speed ratio at a diffuser angle of 20.04°.

3.2 Power coefficient

The experimental result for the power coefficient (C_p) to a base of TSR for the horizontal-axis tidal turbine with a diffuser angle of 20.04° in the flowing tank with a current velocity of 0.7–0.8 m/s is shown in Fig. 11. The data collection was carried out five times, which means 15 000 data points for every data retrieval. The result shows an increase and decrease in C_p as TSR is advanced. The experimental TSR values were 0.9, 1.8, 2.69, 3.59 and 4.49. When the angular speed was 40 rpm at a TSR of 0.9, a C_p of 0.126 was obtained. When the angular speed was increased up to 120 rpm at a TSR of 2.69, the C_p also increased to the maximum of 0.436. An angular speed of >120 rpm displayed a decrease in C_p. The maximum angular speed of the turbine was 200 rpm at a TSR of 4.49 whose C_p was 0.197.

The measurement of the power coefficient uses three measuring tools that have their own uncertainty affected by each value, therefore each point on the graph has different uncertainties. For the power coefficient, the uncertainties were 1.6%, 4.7%, 5.37%, 5.29% and 4.91%, respectively. Meanwhile, the uncertainties of the TSRs were 3.25%, 6.43%, 9.6%, 12.8% and 16%, respectively. By all means, the maximum power coefficient of 20.04 can be between 0.459 and 0.413 at TSR values between 2.95 and 2.43 due to uncertainties of the measuring tools.

Moreover, to reinforce the previous results, the diffuser with an angle of 10.43° was also manufactured and tested experimentally. The diffuser with an angle of 10.43° was tested for five different TSR values as seen in Fig. 12. The TSR values in this experiment were adjusted to be close to the values found in the numerical experiment, which were 1.00, 2.00, 3.00, 4.00 and 4.75. The TSR values obtained were 0.96, 1.91, 2.48, 3.39 and 4.1. If converted into rotational speed values, then the values are 43, 85, 110, 151 and 184 rpm, respectively. The power coefficient (C_p) value obtained tends to increase from a TSR of 0.96 to a TSR of 1.91 and decrease from a TSR of 1.91 to a TSR of 4.1. At a TSR of 1.91, the power coefficient (C_p) reaches its maximum value at 0.303, whereas the minimum power coefficient (C_p) value is found at a TSR of 4.1 and is 0.02.

The value of the power coefficient in this experiment is also influenced by the uncertainty of the measuring instrument. The uncertainty of measuring instruments is the possibility of errors that occur in the data collection process. Each measuring instrument has a different uncertainty. The uncertainty value is also influenced by torque and angular velocity. Therefore, at different values of the power coefficient (C_p) and TSR, the uncertainty values will also be different. The uncertainty values obtained in the power coefficient (C_p) are 1.77%, 3.75%, 4.03%, 4.03% and 4.09%, respectively. Meanwhile, the uncertainty values obtained in the TSRs are 3.49%, 6.83%, 8.83%, 12.10% and 14.75%, respectively. At the highest power coefficient (C_p), the uncertainty value is 3.75%. This shows that the power coefficient (C_p) can be 3.75% smaller or larger than its original value.

Fig. 13 describes that the graph of this experimental result follows the trend of previous studies on horizontal-axis tidal turbines with three blades that have been tested experimentally. It implicitly explains that the methodology of the current work is on the same track as previous works. Batten and Bahaj have published several papers, especially on the experimental study of marine current turbines. An 800-mm rotor diameter with three blades based on NACA 63-8xx sections was experimentally tested with a 1.73-m/s velocity inlet by Batten and Bahaj. From the

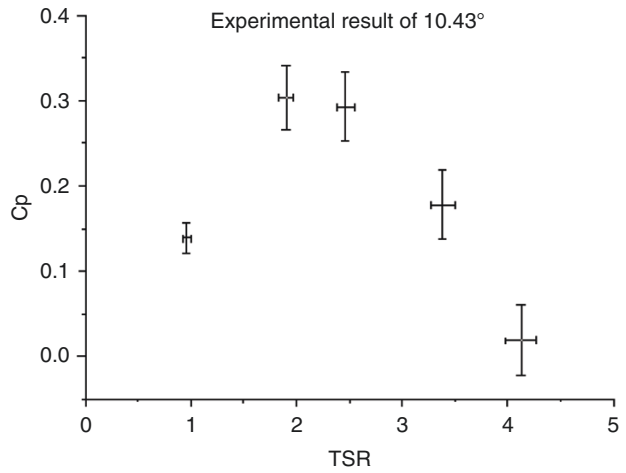

Fig. 12: The power coefficient of the experimental result as a function of the tip speed ratio at a diffuser angle of 10.43°.

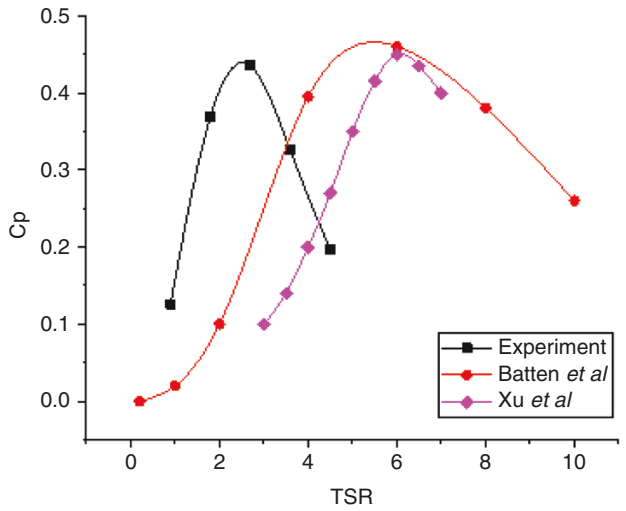

Fig. 13: The experimental result compared with previous studies.

graph, it can be seen that the turbine could generate a rotation of ≤250 rpm at a maximum C_p of 0.45 [26, 27, 31]. Besides, Xu *et al.* have developed a 60-kW horizontal-axis marine current power system. A rotor diameter of 7.2 m with three blades of NACA 63-4 series foil was experimentally tested with a 2-m/s current velocity by Xu *et al.* The graph showed that the maximum C_p is 0.43 at 60 rpm [32].

Even though these two studies above are valid for a bare turbine, this study proposed a diffuser-augmented turbine. However, through the graph in Fig. 13, it can be seen that a diffuser-augmented turbine with a small rotor and low free-stream velocity can produce more rpm to achieve the maximum power coefficient.

4 Comparison between experimental and numerical methods

The key finding of the experimental campaign was the validation of the computational fluid-dynamic model for the estimation of the power output of a diffuser-augmented device. The model has been shown to represent the power coefficient of the device well for both efficiencies tested.

The limitations of the current model have been solved with some approaches. Even though the artificial currents were created by rotating two ship propellers using an electric motor drive, a straightener located in front of the turbine was utilized to straighten the flow before hitting the turbine. A simple correction for the tank length of 2.44 m, which is categorized as short, to the reverse flow in the flowing tank has been corrected by building the circulating current. It should be noted that the accuracy of the section data is the prime driver of the model fidelity as with any CFD model. It is therefore of significant importance to ensure as far as possible that the data are accurate for the flow conditions that will be experienced by the rotor at all points.

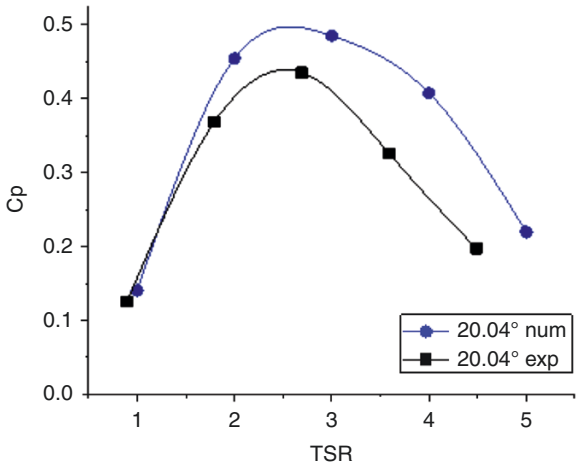

Fig. 14: The comparison of power coefficients of the numerical and experimental results as a function of the tip speed ratio at a diffuser angle of 20.04°.

The CFD method was shown to predict the optimum design of the diffuser-augmented horizontal-axis tidal turbine. The work was to compare the turbine performance with seven diffuser angles. This was primarily due to shortening the processing time; the simplest CFD model was applied as a prediction result of the turbine performance in the numerical method. It is therefore recommended that further work on a more complex model be conducted to ascertain the turbulence structure generated within the diffuser by the turbine. An empirical relation can then be arrived at to represent the complex turbulence model with unsteady state within the CFD model. The model, despite its limitation, has been shown to be accurate for the prediction of device performance at the design stage.

The results seen in this section show that both diffusers can maintain device performance at an inlet velocity of 0.7 m/s. Both diffusers are able to increase the current velocity by ≤1 m/s. Fig. 12 displays the comparison of numerical and experimental outputs on a diffuser with a 20.04° angle. It displays that the experimental C_p value for a diffuser angle of 20.04° approached the numerical values for TSR values of ≤2 then became slightly lower than the numeric values. At a TSR of 1, both start from a C_p that is insignificantly different. The numerical C_p result here is not the normalized C_p to the peak C_p, but the real one instead. The maximum C_p values of the numerical and experimental results are 0.485 and 0.436, respectively. The maximum rpm of the numerical result occurs at a TSR of 5 with 222 rpm. Meanwhile, the maximum rpm of the experimental result occurs at a TSR of 4.5 with 200 rpm.

For the diffuser with an angle of 10.43°, both numerical and experimental values have the same tendency as seen in Fig. 15, which tends to increase from TSR values of 1.00 to 2.00 and decrease from TSR values of 3 to 4.75, referring to the numerical values. The inflection points of the two graphs are also the same, located between TSR values of 2.00 and 3.00, which refers to the

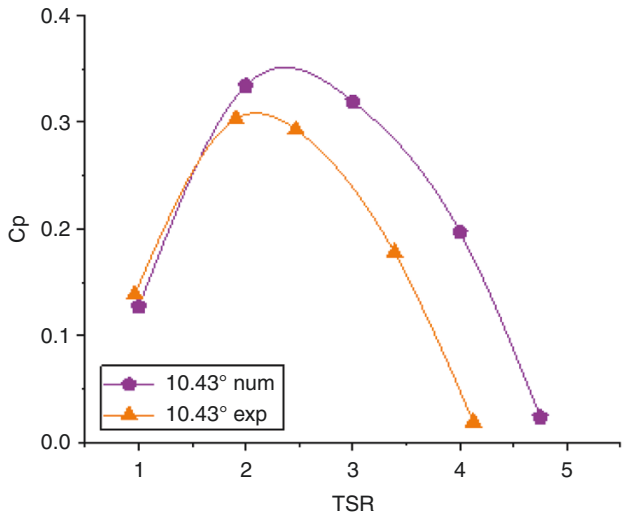

Fig. 15: Comparison of power coefficient on numerical and experimental results as a function of the tip speed ratio at a diffuser angle of 10.43°.

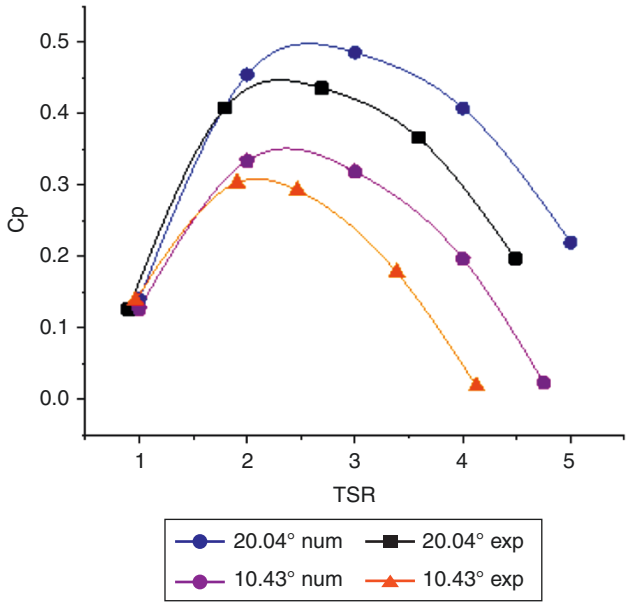

Fig. 16: The comparison of power coefficients in numerical and experimental results as a function of the tip speed ratio at both diffuser angles.

numerical values. The highest and lowest values also exist at the same point, which is located at TSR values of 2.00 and 4.75, but the values obtained are not identical. The maximum power coefficients (C_p) of the numerical and experimental results are 0.334 at 89 rpm and 0.303 at 85 rpm, respectively. The maximum rotational speed of the numerical results can reach 212 rpm, whereas for the experimental results, the maximum rotational speed is 184 rpm.

The smallest data difference in the two studies occurred at a TSR of 2.47 with a power coefficient (C_p) of 0.026 (8.21%). But, when compared with numerical data for a TSR of 3.00, the difference between both TSR values is a little too large. As a more accurate comparison, the second data can be used as a reference because the difference between the TSR in the numerical and experimental methods is only 0.09. So, in the second data, the difference obtained is 0.031 (9.3%) and can be said to be the smallest difference in these experimental data. In the fourth-to-last data, the difference between the numerical and experimental values is 0.019 (9.67%) at a TSR of 3.39 and 0.005 (19.35%) at a TSR of 4.13. Overall, the values obtained in the experimental investigation tend to be smaller than those of the numerical investigation. However, this does not happen when the TSR is close to 1.00, referring to the numerical investigation. As the numerical approach to a TSR of 1.00, the experimental value is slightly higher by 0.01 (9.28%) compared to the numerical value. However, this can still be said to be reasonable because the value of the difference is quite small.

Comparing the difference between the numerical and experimental results at an angle of 20.04° with 10.43° can evaluate the accuracy of the experimental process carried out as shown in Fig. 16. At TSR values of 2.00–5.00, the two angles have differences with a similar tendency. The experimental results produced at each angle are always smaller than the numerical values. The smallest difference equally occurs in the second TSR. For a diffuser angle of 10.43°, the difference between the numerical and experimental values is 0.031, whereas for a diffuser angle of 20.04°, the difference between the numerical and experimental values is 0.047. At the third-to-last TSR, the difference tends to increase. In the first to second TSRs, both the experimental angles of 10.43° and 20.04° have greater experimental values. For the diffuser with an angle of 20.04°, the difference is so small that the two lines almost touch, whereas for the diffuser with an angle of 10.43°, the difference is slightly larger and intersects the numeric line.

From the comparison of data on the two diffusers, it can be said that the greater the angle of the diffuser, the greater the efficiency obtained, which is in an agreement with the computational study [21, 22]. This can be caused by the larger mass flow rate at an angle of 20.04°. The larger mass flow rate is due to the larger pressure difference. This causes the water to flow faster for the diffuser with an angle of 20.04° and makes the diffuser with an angle of 20.04° have better efficiency.

The efficiency difference of the diffusers in experimental and numerical results can be attributed to several possible factors. In the current experiment, mechanical losses caused by friction between the bearing and turbine shaft and the existence of bearings, pulleys, diffuser foundation and turbine foundation that reduce the efficiency were not taken into account in the computational work. The presence of diffuser and turbine foundations can interfere with the fluid flow, which will generate different results from the velocity profile shown in the numerical results. Moreover, the uncertainty of measuring instruments cannot be neglected. The limitation of the test area as presented in the blockage ratio is one of the obstacles in this experiment.

5 Conclusions

The experimental method was conducted to validate the numerical model. Diffusers with angles of 10.43° and 20.04° were manufactured and tested in a flowing tank with an inlet velocity of 0.7 m/s. The power coefficients were compared between the numerical and experimental results. With all limitations and some approaches, on the diffuser with an angle of 20.04°, it was found that experimentally the maximum efficiency of the tidal turbine was 43.6% with 120 rpm, whereas numerically the maximum efficiency could reach ≤48.5% with 133 rpm. The difference between the numerical and experimental results for the 20.04° diffuser angle was 4.7%; for the diffuser with an angle of 10.43°, the maximum efficiency was ≤30.3% with 85 rpm, whereas in the numerical results, the maximum efficiency could reach ≤33.4% with 89 rpm. The difference between the numerical and experimental results for the 10.43° diffuser angle was 3.1%.

The test programmes carried out at Universitas Indonesia on the diffuser-augmented horizontal-axis tidal turbine model and the developed numerical model have presented great suitability with experiments. In conclusion, the CFD model with the k-epsilon turbulence model in the steady state is considered to be able to represent similar phenomena to the experimental investigations in terms of applying the numerical results for preliminary design investigations and parametric studies. However, to further advance the agreement between numerical and experimental results, it requires several improvements in boundary conditions and consideration of mechanical losses such as the existence of bearings, pulleys and foundations as occurred in experimental methods. Nevertheless, by observing the trend in Fig. 14, it is concluded that this numerical approach might be considered satisfactorily representative an application for the modelling of multi-objective optimization carried out by Ambarita *et al.* [21, 22].

Acknowledgements

Conceptualization: E.E.A. and H.; methodology: E.E.A., R.A. and R.I.; software: E.E.A.; validation: E.E.A., R.A. and H.; writing—original draft preparation: E.E.A. and R.A.; writing—review and editing: E.E.A., H. and R.I.; supervision: H.

Funding

This research was funded by Kementerian Riset dan Teknologi / Badan Riset dan Inovasi Nasional (Kemenristek/BRIN) through Publikasi Dasar Unggul Perguruan Tinggi (PDUPT) grant program, grant number NKB-197/UN2.RST/HKP.05.00/2021.

Conflict of interest statement

None declared.

References

[1] Garnes G, Jensen JW, Rogne A. Upstream blockage and downstream wake flow of a wind turbine. *Bachelor's thesis*. Energy Technology Bergen, Western Norway University of Applied Sciences, Bergen, Norway, 2020. https://hvlopen.brage.unit.no/hvlopen-xmlui/bitstream/handle/11250/2679277/Garnes_Jensen_Rogne.pdf?sequence=1 (14 April 2022, date late accessed).

[2] Shetty C, Priyam A. A review on tidal energy technologies. *Material Proceedings*, 2021, 56:2774–2779.

[3] Lavidas G, Kamranzad B. Assessment of wave power stability and classification with two global datasets. *International Journal of Sustainable Energy*, 2021, 40:514–529.

[4] Li M, Luo H, Zhou S, *et al.* State-of-the-art of the flexibility and feasibility of emerging offshore and coastal ocean energy technologies in East and Southeast Asia. *Renewable and Sustainable Energy Reviews*, 2022, 162:112404.

[5] Kozarcanin S, Andresen GB, Greiner M. Impact of climate change on the backup infrastructure of highly renewable electricity systems. *Journal Sustainable Development of Energy Water and Environment Systems*, 2018, 6:710–724.

[6] Amoo LM. Aperiodic tidal data resource assessment and LCOE analysis of selected area in Nigeria. *Clean Energy*, 2018, 2:45–57.

[7] Huang B, Zhao B, Wang L, *et al.* The effects of heavy motion on the performance of a floating counter-rotating type tidal turbine under wave-current interaction. *Energy Conversion and Management*, 2022, 252:115093.

[8] Noorollahi Y, Ghanbari S, Tahani M. Numerical analysis of a small ducted wind turbine for performance improvement. *International journal of Sustainable Energy*, 2020, 39:290–307.

[9] Nunes MM, Mendes RC, Oliveira TF, *et al.* An experimental study on the duct-enhanced propeller hydrokinetic turbines. *Renewable Energy*, 2019, 133:840–848.

[10] Agromayor R, Nord LO. Preliminary design and optimization of axial turbines accounting for diffuser performance. *International Journal of Turbomachinery, Propulsion and Power*, 2019, 4:32.

[11] Mehmood N, Liang Z, Khan J. Diffuser augmented horizontal axis tidal current turbines. *Research Journal of Applied Sciences, Engineering and Technology*, 2012, 4:3522–3532.

[12] Cresswell NW. The generation potential of diffuser augmented tidal stream turbines. *Master thesis*. Durham University, UK, 2015. http://etheses.dur.ac.uk/10980/ (5 May 2021, date last accessed).

[13] Elbatran AYO, Ahmed Y. Augmented diffuser for horizontal axis marine current turbine. *International Journal of Power Electron Drive System*, 2016, 7:235–245.

[14] Cresswell NW, Ingram GL, Dominy RG. The impact of diffuser augmentation on a tidal stream turbine. *Ocean Engineering*, 2015, 108:155–163.

[15] Mehmood N, Liang Z, Khan J. Study of NACA 0015 for diffuser design in tidal current turbine applications. *International Journal of Engineering*, 2012, 25:373–380.

[16] Mehmood N, Liang Z, Khan J. CFD study of NACA 0018 for diffuser design of tidal current turbines. *Research Journal of Applied Sciences Engineering and Technology*, 2012, 4:4552–4560.

[17] Shahsavarifard M, Bibeau EL, Chatoorgoon V. Effect of shroud on the performance of horizontal axis hydrokinetic turbines. *Ocean Engineering*, 2015, 96:215–225.

[18] Song K, Wang WQ, Yan Y. Numerical and experimental analysis of a diffuser-augmented micro-hydro turbine. *Ocean Engineering*, 2019, 171:590–602.

[19] Kyozuka Y, Sueyoshi M, Obara K, *et al.* A floating/submersible tidal current power generator applicable in low speed tidal flow. In: *International Conference of Grand Renewable Energy 2018 Proceedings*, Yokohama, Japan, 17–22 June 2018. https://www.jstage.jst.go.jp/article/gre/1/0/1_235/_pdf (4 May 2021, date last accessed).

[20] Sun H, Kyozuka Y. Analysis of performances of a shrouded horizontal axis tidal turbine. In: *2012 Oceans—Yeosu*, Yeosu, South Korea, 21–24 May 2012, 1–7, Publisher IEEE. https://doi.org/10.1109/OCEANS-Yeosu.2012.6263455 (4 May 2021, date last accessed).

[21] Ambarita EE, Harinaldi H, Nasruddin N, *et al.* A study on diffuser augmentation of a tidal turbine. *Journal of Advanced Research in Fluid Mechanics and Thermal Sciences*, 2021, 83:170–177.

[22] Ambarita EE, Harinaldi H, Nasruddin N. Computational study on multi-objective optimization on the diffuser augmented horizontal axis tidal turbine. *Journal of Marine Science & Technology*, 2021, 26:1237–1250.

[23] Sakaguchi D, Kyozuka Y. Design of shrouded tidal current turbine by multi-objective optimization. In: *International Conference of Grand Renewable Energy 2018 Proceeding*, Yokohama, Japan, 17–22 June 2018.

[24] Zhang D, Ding L, Huang B, *et al.* Optimization study on the blade profiles of a horizontal axis tidal turbine based on BEM-CFD model. *China Ocean Engineering*, 2019, 33:436–445.

[25] Huang B, Chen XM, Zhang D, *et al.* Multi-objective optimization of blade profiles for a horizontal axis tidal turbine. *IOP Conference Series: Earth and Environmental Science*, 2018, 163:012086.

[26] Bahaj AS, Molland AF, Chaplin JR, *et al.* Power and thrust measurements of marine current turbines under various

hydrodynamic flow conditions in a cavitation tunnel and a towing tank. *Renewable Energy*, 2007, 32:407–426.

[27] Batten WMJ, Bahaj AS, Molland AF, *et al*. The prediction of the hydrodynamic performance of marine current turbines. *Renewable Energy*, 2008, 33:1085–1096.

[28] ANSYS Inc. *2019 ANSYS Fluent Theory Guide*. 2019. http://www.ansys.com (12 April 2021, date last accessed).

[29] Schluntz J, Willden RHJ. The effect of blockage on tidal turbine rotor design and performance. *Renewable Energy*, 2015, 81:432–441.

[30] Hartono MU. Analisa Pengaruh Diameter Pulley Terhadap Kinerja Engine pada Power Double Thresher. *Bachelor thesis*. UPT, Perpustakaan, Universitas Mataram, Mataram City, Indonesia, 2017. http://eprints.unram.ac.id/id/eprint/1203 (12 April 2021, date last accessed).

[31] Batten WMJ, Bahaj AS, Molland AF, *et al*. Hydrodynamics of marine current turbines. *Renewable Energy*, 2006, 31:249–256.

[32] Xu QK, Liu HW, Lin YG, *et al*. Development and experiment of a 60-kW horizontal-axis marine current power system. *Energy*, 2016, 88:149–156.